Radiocarbon in the Antarctic Ice: The Formation of the Cosmic Ray Muon Component at Large Depths

A. V. Nesterenok and V. O. Naidenov

Ioffe Physical-Technical Institute, Russian Academy of Sciences,
Politekhnicheskaya ul. 26, St. Petersburg, 194021 Russia
e-mail: alex-n10@yandex.ru

Abstract—This study is devoted to the production of ^{14}C by the secondary cosmic radiation in polar ice. The radiocarbon production in the reactions caused by the nuclear-active and muon components is considered. The data on ^{14}C from the Vostok and Taylor Dome Antarctic boreholes are analyzed. The ^{14}C concentration values at depths larger than the firn–ice boundary by a factor of 2–3 can be explained by a deep production of radiocarbon in the reactions caused by the cosmic radiation muon component.

1. INTRODUCTION

Oxygen concentration in polar ice is determined during two processes: trapping of ^{14}C together with air in the process of ice deposition and radiocarbon production by the secondary cosmic radiation in a glacier body (in situ production). The amount of atmospheric radiocarbon is estimated proceeding from the amount of air in an ice sample, CO_2 percentage, and $^{14}C/^{12}C$ ratio during the period corresponding to the air age in a sample. Radiocarbon production by the nuclear-active component of the cosmic radiation takes place in the upper glacier layer with a thickness of several meters of the water equivalent. Having been produced, ^{14}C atom oxidizes to CO and CO_2. The effectiveness of ^{14}C retention by the ice crystal lattice is still unclear. For ice samples from the GISP2 Greenland borehole, the theoretical calculation of the ^{14}C concentration is similar with the experimental data in an order of magnitude [Lal et al., 2005]. At the same time, for ice samples from the Vostok and Taylor Dome Antarctic boreholes, the experimental concentrations are much lower than the calculated values [Lal et al., 2001]. Lal et al. [2001] assumed that the deficit of ^{14}C is related to the processes of sublimation, transport, and fragmentation of snow granules caused by air flows in the upper firn layers. The loss of ^{14}C can also be caused by gas diffusion into firn cavities with the following escape into the atmosphere [Smith et al., 2000]. The effectiveness of ^{14}C retention by the ice crystal lattice makes it difficult to interpret experimental data.

In the present work, we analyze the data on ^{14}C in the Vostok [78°28′ S, 106°48′ E] and Taylor Dome (77°47′ S, 158°43′ E) boreholes published in [Lal et al., 2001]. We indicated that the reactions caused by the cosmic radiation muon component mainly contribute to the radiocarbon concentration in deep ice samples.

2. REVIEW OF ^{14}C PRODUCTION PROCESSES IN ICE

2.1. Production of ^{14}C by the Nuclear-Active Component of Cosmic Rays

The reactions of oxygen atom chipping by energetic neutrons are the reactions of ^{14}C production in ice by the nuclear-active component of cosmic rays. The semiempirical method [Lal, 1991; Desilets and Zreda, 2003; Desilets et al., 2006] is used to calculate the radionuclide production rate in rock (ice) at a given latitude and longitude. The dependence of the production rate (P_h) on depth h is considered to be as follows:

$$P_h = P_0 e^{-\rho h/\Lambda_h},$$

where P_0 is the surface production rate, Λ_h is the neutron free path in a target substance (160 g cm^{-2} for ice), and ρ is the density of a medium. The equilibrium radionuclide concentration in rock samples is used to estimate the surface production rate of this radionuclide (P_0) (see, e.g., [Jull et al., 1994]). The P_0 value is recalculated for different geomagnetic latitudes and heights above sea level.

2.2. Production of ^{14}C by High-Energy Muons

Propagating in a substance, high-energy muons generate cascades of the secondary particles: δ-electrons, e^-e^+ pairs, electromagnetic cascades, and hadrons. The set of reactions, caused by the secondary particles and during which a given radionuclide is generated, is described by the differential cross section σ(E) (E is the muon energy). The number of radionuclide atoms, produced in a unit volume per unit time in a target at depth h, is:

$$P_{\mu f}(h) = \iint dE d\Omega I(h, \theta)\sigma(E)N,$$

where N is the concentration of nuclei-targets, $I(h, \theta)$ is the muon flux at depth h in direction θ from the vertical, σ(E) is the radionuclide production cross section during the secondary processes caused by muon with energy E, and dΩ is the solid angle differential. The dependence of the cross section on energy E is set in the form [Heisinger et al., 2002a]:

$$\sigma(E) = \sigma_0 E^{\alpha},$$

where $\sigma_0 = \sigma(1\text{ GeV})$, the parameter E value corresponds to the muon energy in GeV, and exponent α is about 1.

2.3. Production of ^{14}C in the Reactions of Slow μ^- Trapping

At the end of its motion, negative muon is trapped by the outer shell of one of the atoms in a medium. Muon very rapidly (during about 10^{-13} s) descends to the 1s energy level and subsequently decays into electron and neutrino or reacts with a nucleus [Measday, 2001]. In the second case, a produced excited nucleus passes into the ground state, emitting γ, n, p, and α particles. For the ^{14}C production rate by stopping muons at depth h in a target, we have the following expression:

$$P_{\mu^-}(h) = R_{\mu^-}(h)f_0 f_D f^*(^{14}\text{C}),$$

where $R_{\mu^-}(h)$ is the number of negative muons stopping in a unit volume per unit time; f_0 is the probability of negative muon trapping by atom; f_D is the fraction of muons reacting with nuclei; and $f^*(^{14}\text{C})$ is the probability of the reaction channel producing the considered radionuclide. The $R_{\mu^-}(h)$ function is:

$$R_{\mu^-}(h) = -f_{\mu^-}\frac{dI(h)}{dh},$$

where $I(h)$ is the muon flux at depth h in a target, and $f_{\mu^-} = 0.44$ is the fraction of negative muons [Heisinger et al., 2002b].
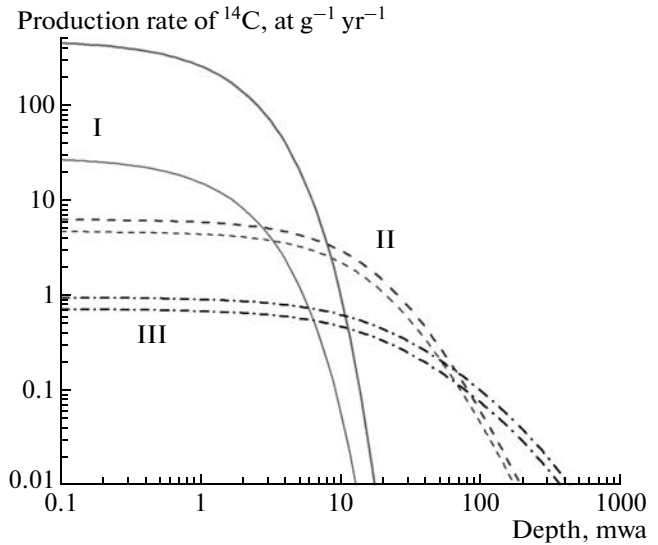

Fig. 1. The ^{14}C production rates in an ice target for geomagnetic latitudes of λ > 60°: by the nuclear-active component of the cosmic radiation (I), in the reactions of negative muon trapping (II), and by high-energy muons (III). The lower and upper curves in each group correspond to sea level and the Vostok station height (3.5 km), respectively. The depth in mwa is plotted on the abscissa (mwa = 100 g cm^{-2}).

2.4. Concentration of ^{14}C in Ice Samples

Figure 1 presents the radiocarbon production rates in ice by different components of the secondary cosmic radiation. The lower dependence in each group of curves corresponds to sea level; the upper, to the Vostok station height (3.5 km). The radiocarbon production in the reactions, caused by the nuclear-active component of the cosmic radiation, is substantial at shallow depths, up to 10 m of the water equivalent (mwa = 100 g cm^{-2}). Radiocarbon is produced by the muon component at depths of up to 100 and more mwa. In a first approximation ($P_h \propto e^{-h/\Lambda_h}$, $P_{\mu^-} \propto e^{-h/\Lambda_{\mu^-}}$, and $P_{\mu f} \propto e^{-h/\Lambda_{\mu f}}$, where $\Lambda_h = 1.6$ mwa, $\Lambda_{\mu^-} = 15$ mwa, and $\Lambda_{\mu f} = 44$ mwa), radiocarbon is mainly produced in the upper glacier layer with a thickness of several tens of mwa.

The concentration of in situ produced radiocarbon for ice accumulation regions and in the absence of loss during ice formation is:

$$n(h) = \int_0^t dt' P(h'(t'))e^{-\lambda(t-t')},$$

where t is the age of ice at depth h, P(h) is the radionuclide production rate, λ is the decay constant, h'(t') is the dependence of the sampled ice layer depth on
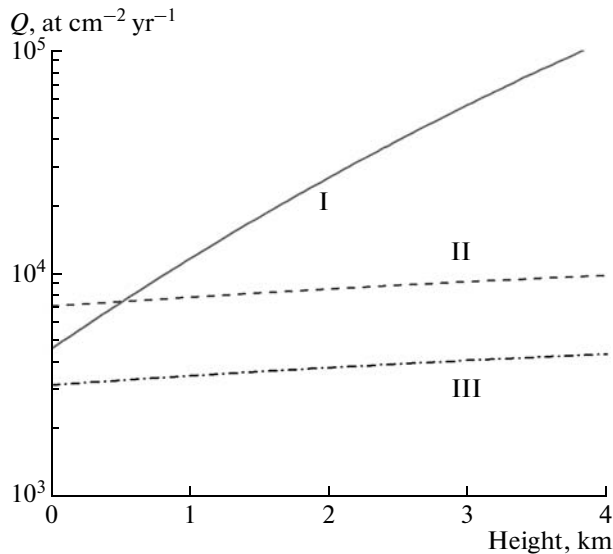
Q, at cm^{-2} yr^{-1}

Fig. 2. The dependence of the radiocarbon production integral rates on the glacier surface height above sea level for geomagnetic latitudes of $\lambda > 60°$: by the nuclear-active component of the cosmic radiation (I), in the reactions of negative muon trapping (II), and by high-energy muons (III). The ^{14}C integral production rate in at cm^{-2} yr^{-1} is plotted on the ordinate.

time, and the form of the $h'(t')$ function depends on the ice accumulation rate and the flow of the overlying glacier layers. For depths much smaller than glacier thickness, the $h(t) = s\rho t$ equality holds, where s is the average sedimentation rate in equivalent centimeters of ice per year, and ρ is the ice density [Reeh, 1989]. Neglecting the radionuclide production at large depths, we have:

$$n(h) = \left(\frac{Q_h}{s\rho} + \frac{Q_{\mu^-}}{s\rho - \Lambda_{\mu^-}\lambda} + \frac{Q_{\mu f}}{s\rho - \Lambda_{\mu f}\lambda} \right) e^{-\lambda t}, \quad (1)$$

where s is the average ice accumulation rate during the period of radionuclide production; Q_h, Q_{μ^-}, and $Q_{\mu f}$ are the integral rates of radionuclide production by nuclear-active and muon components, respectively; and $Q = \int_0^\infty P(h)dh$. Expression (1) has a sense for $s\rho > \lambda\Lambda_{\mu f} \approx 0.5$ g cm^{-2} yr^{-1}. Figure 2 presents the depen-

Table 1. Integral rates of ^{14}C production by the cosmic radiation components for Vostok and Taylor Dome stations (the Q values are given in 10^3 at cm^{-2} yr^{-1})

Station	Height, km	$Q_{\mu f}$	Q_{μ^-}	Q_h	Q_Σ
Taylor Dome	2.4	4.0	8.8	37	50
Vostok	3.5	4.3	9.5	80	94

dences of the radionuclide production integral rates on the glacier height; Table 1, the values of these quantities for the heights of Vostok and Taylor Dome stations. The contribution of the muon component to the radiocarbon production process is about 15 and 25% for the Vostok and Taylor Dome borehole samples, respectively.

The concentration of the radionuclide produced at depths larger than a certain depth h_0 is:

$$n(h) = \int_{t_0}^{t} dt' P(h'(t')) e^{-\lambda(t-t')}, \quad (2)$$

where t_0 is the instant corresponding to depth h_0. The depth of the considered ice samples from the Vostok borehole is $h < 400$ m, which is much smaller than the glacier thickness ($H = 3.7$ km). In an approximation of constant ice accumulation rate and glacier height accurate to small quantities about h/H, we have $h'(t') = ht'/t$ (based on [Reeh, 1989]).

3. ANALYSIS OF DATA ON ^{14}C FROM VOSTOK AND TAYLOR DOME BOREHOLES, ANTARCTICA

3.1. The Main Parameters of Ice Formation and Climatic Conditions at Vostok and Taylor Dome Stations

Table 2 presents the climatic conditions and parameters of ice formation for Vostok and Taylor Dome stations [Salamatin and Lipenkov, 2008; Steig et al., 1998]: T is temperature; s is the sedimentation rate in equivalent centimeters of ice per year; h_c is the depth of the firn–ice boundary in meters; t_c and ρ_c are the ice age and density corresponding to depth h_c, respectively; and the density values are normalized to the ice density ($\rho = 0.92$ g cm^{-3}).

For the Vostok and Taylor Dome boreholes, the depth of the firn–ice boundary (h_c) is 99 and 74 m, respectively. Assuming that the firn structure is constant for a specified area, we use the following expression for estimating the firn–ice boundary depth (h_c') under the conditions of the surface temperature (T') and ice accumulation rate (s') according to [Salamatin and Lipenkov, 2008]:

$$h_c' = h_c \left(\frac{s'}{s} \right)^{\frac{1}{1+\alpha}} e^{\frac{Q}{R(1+\alpha)}\left(\frac{1}{T} - \frac{1}{T'}\right)}, \quad (3)$$

where h_c is the specified depth of the firn–ice boundary under the corresponding firn temperature (T) and accumulation rate (s), $R = 8.314$ J (mol K)$^{-1}$, $Q = 63.6$ kJ mol^{-1}, and $\alpha = 3.5$. The model error of the expression for h_c' is about 3%. Note that the h_c' value weakly depends on the parameter s' variations: a

Table 2. Climatic conditions and ice formation parameters for Vostok and Taylor Dome stations

Station	T, K	s, cm yr^{-1}	h_c, m	t_c, years	ρ_c
Vostok	216	2.15	99	3300	0.91
Taylor Dome	231	5.5	74	1000	0.9

change in the accumulation rate by 10% results in an only 2%-change in the h'_c value.

3.2. Experimental Data

Tables 3 and 4 (columns 1−6) present the data for the considered ice samples from the Vostok and Taylor Dome boreholes. Columns 1 and 2 of both tables present the sample codes and depths, respectively [Lal et al., 2001].

Column 3 of Table 3 presents the age of ice samples from the Vostok borehole according to the EGT chronology [Jouzel et al., 1993], which was used by Lal et al. [2001] during the experimental data processing (the age was counted off from 1950). The sample age according to the GT4 chronology [Petit et al., 1999] is presented in parentheses in the case of a substantial difference. A difference in the data can be a measure of the dating error (about 5−7%). Column 4 presents the average ice accumulation rates (s) during the periods corresponding to the sample age in equivalent centi-

meters of ice per year [Lal et al., 2001]. Column 5 presents the relative temperature variations during the considered periods [Petit et al., 1999]. The period of data averaging over temperature is 3000−5000 years, which corresponds to the ice age at the firn−ice boundary in the order of magnitude. The indicated error characterizes the statistical scatter of data relative to the average value and corresponds to one standard deviation.

Column 3 of Table 4 presents the age of ice samples from the Taylor Dome borehole according to the st9507 chronology [Grootes et al., 1994], and the age according to the EDC1 chronology [Monnin et al., 2004] is given in parentheses; the ice accumulation rates are presented in column 4 [Lal et al., 2001]. Column 5 presents the relative temperature variations reconstructed using the δ^{18}O data, where $d\delta^{18}O/dT = 0.5\%o$ C^{-1}, and the data from [Grootes et al., 1994; Steig et al., 1998] were used; the data averaging period is about 1000 years.

Columns 6 of both tables present the experimental values of the ^{14}C concentrations [Lal et al., 2001]. The experimental method for determining ^{14}C activity included ice sample melting, which makes it possible to extract all gases included in ice. Lal et al. [2001] made a correction for atmospheric radiocarbon and the secondary production during ice sample storage. The data were also corrected for radioactive

Table 3. Experimental data and calculation results for the Vostok borehole samples

1	2	3	4	5	6	7	8	9
Sample code	Depth, m	Age, ka, EGT (GT4)	s, cm yr^{-1}	ΔT, K	^{14}C, exper., 10^3 at g^{-1}	^{14}C, complete calculation, 10^3 at g^{-1}	h_c, m	^{14}C, calculation $h > h_c$, 10^3 at g^{-1}
I001	7	0.13	2.2	0	>0.7 ± 0.10	35 ± 6	−	−
D3	10	0.19	2.1	0	3.2 ± 0.10	42 ± 7	−	−
I006	25	0.55	2.1	0	0.05 ± 0.07	48 ± 8	−	−
O11	56	1.55	2.1	0	0.18 ± 0.06	51 ± 8	−	−
I003	60	1.7	2.1	0	0.62 ± 0.06	51 ± 8	−	−
I005	70	2.1	2.1	0	0.58 ± 0.08	52 ± 8	−	−
V112	112	3.8 (4.0)	2.2	0	6.33 ± 0.16	50 ± 8	99	0.25 ± 0.08
L1	116	4.0 (4.2)	2.2	0	4.41 ± 0.13	50 ± 8	99	0.3 ± 0.1
L8	211	8.3 (8.7)	2.3	−0.1 ± 0.6	2.59 ± 0.12	45 ± 8	100	1.4 ± 0.5
O16	266	10.8 (11.3)	1.8	−0.3 ± 0.6	1.99 ± 0.18	59 ± 10	96	1.8 ± 0.7
I002	267	10.8 (11.4)	1.8	−0.4 ± 0.6	4.82 ± 0.15	59 ± 10	96	1.8 ± 0.7
I004	297	12.4 (13.1)	1.8	−1.6 ± 1.5	6.46 ± 0.24	59 ± 10	100	2.0 ± 0.8
L7	333	14.6 (15.3)	1.6	−3.5 ± 0.8	3.72 ± 0.3	66 ± 11	104	2.4 ± 1.0
0I007	396	19.5 (20.3)	1.3	−7.8 ± 0.6	5.07 ± 0.17	83 ± 14	120	3.3 ± 1.5

Table 4. Experimental data and calculation results for the Taylor Dome borehole samples

1	2	3	4	5	6	7	8	9
Sample code	Depth, m	Age, ka, st 9507 (EDC1)	s, cm yr^{-1}	ΔT, K	^{14}C, exper., 10^3 at g^{-1}	^{14}C, complete calculation, 10^3 at g^{-1}	h_c, m	^{14}C, calculation $h > h_c$, 10^3 at g^{-1}
O7	1.5–1.9	0.01	5.4	0	0.40 ± 0.04	2.6 ± 0.5	–	–
O10	4.0–4.3	0.08	5.7	0	0.11 ± 0.04	4.8 ± 0.9	–	–
L6	30–31	0.52	5.8	0	2.46 ± 0.07	8.8 ± 1.4	–	–
L4	54–55	0.97	4.9	0	0.21 ± 0.07	11.0 ± 1.7	–	–
L3	84–85	1.65	5.6	0	0.56 ± 0.06	10.0 ± 1.5	74	0.09 ± 0.03
O20	200–201	4.2 (3.6)	5	1.0 ± 1.2	1.18 ± 0.11	11.0 ± 1.8	70	0.70 ± 0.24
O19	251–252	5.5 (5.4)	4.8	1.5 ± 1.5	0.73 ± 0.12	11.5 ± 1.9	69	0.8 ± 0.3
O22	327–328	8.3 (8.2)	1.5	3.3 ± 0.8	1.18 ± 0.18	39 ± 6	50	1.4 ± 0.5
O24	355–356	10.7 (9.2)	0.84	3.6 ± 1.0	1.91 ± 0.17	79 ± 15	50	1.9 ± 0.7

decay. The age error can result in an additional error of about 10%.

3.3. Results of ^{14}C Concentration Calculation

The results of calculating the concentrations of in situ produced ^{14}C for the Vostok and Taylor Dome boreholes are presented in columns 7 of Tables 3 and 4 and in Figs. 3a and 3b, respectively. The approximation of the firn density dependence on depth from [Salamatin and Lipenkov, 2008] was used in the calculations.

The firn–ice boundary depths (h_c), calculated based on expression (3), are presented in columns 8 of both tables. For the last two samples from Taylor Dome (O22 and O24), the average ice accumulation rate was set to be 1.5 ± 0.5 cm yr^{-1}. The data on $\delta^{15}N$ from Taylor Dome indicate that the firn layer thickness decreased by a factor of 1.5–2 during the period 8–12 ka BC [Monnin et al., 2004], which agrees with our result to within the error. Columns 9 of both tables and Figs. 3a and 3b present the results of calculating the concentration of ^{14}C produced at depths larger than the firn–ice boundary depth (h_c). All presented data on ^{14}C were corrected for radioactive decay; i.e., the $e^{-\lambda t}$ multiplier was ignored in expressions (1) and (2) for concentration (t is the sample age).

The errors indicated in the tables and figures correspond to those of the radiocarbon production rates. For the reactions caused by the nuclear-active component and for the reactions of negative muon trapping, the error was 20%; for the reactions caused by muons with higher energies, 60% [Lal, 1991; Heisinger et al., 2002a, 2002b; Desilets et al., 2006]. Since radiocarbon at large depths is produced due to the reactions caused by muons, the corresponding concentration error is 40–60%. The concentration error caused by the h_c inaccuracy is insignificant as compared to the reaction cross section error:

$$\frac{\partial n}{\partial h_c}\Delta h_c / n \approx \frac{P(h_c)\Delta h_c}{\int\limits_0^\infty P(h)dh} \approx \frac{\Delta h_c}{h_c} \le 10\%.$$

4. DISCUSSION

As was mentioned above, radiocarbon produced in a glacier upper layer is partially lost by the ice crystal lattice during snow sublimation and recrystallization [Lal et al., 2001] and owing to gas diffusion into firn air cavities [Smith et al., 2000] The ^{14}C loss in layers that passed the stage of firn transformation into ice becomes insignificant. Thus, the following inequality is satisfied:

$$n_{\text{prod}} \ge n_{\text{exp}} \ge n_{\text{prod} \ge h_c},$$

where n_{prod} is the concentration of ^{14}C produced by the cosmic radiation, n_{exp} is the experimental concentration value corrected for atmospheric radiocarbon, and $n_{\text{prod} \ge h_c}$ is the concentration of ^{14}C produced below the firn–ice boundary. Figures 3a and 3b present the results of calculating the n_{prod} and $n_{\text{prod} \ge h_c}$ values. For all ice samples, the $n_{\text{prod} \ge h_c}$ values are not larger than the experimental values to within the error. For samples L1, V112 (Vostok), and L3 (Taylor Dome), the $n_{\text{prod} \ge h_c}$ values are small because the sample depth is shallow.

Cosmic ray intensity is one of the main parameters responsible for ^{14}C concentration in polar ice. Cosmic
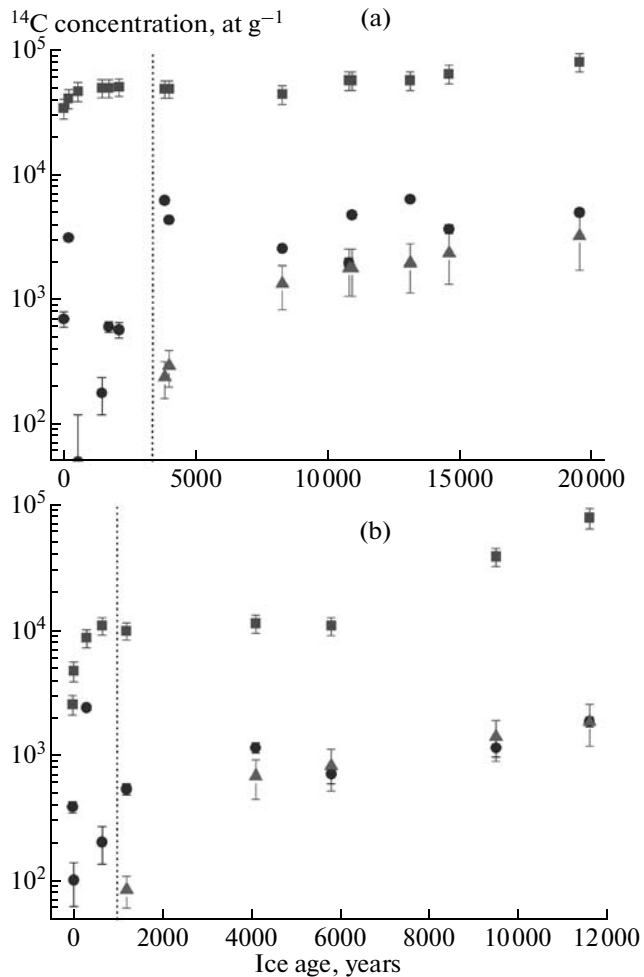
^{14}C concentration, at g^{-1} (a)

Fig. 3. The experimental data and calculation results for the (a) Vostok and (b) Taylor Dome stations: the experimental data corrected for radioactive decay (circles) [Lal et al., 2001]; the calculated concentration ignoring the ^{14}C loss during ice formation (squares); the concentration of radiocarbon produced at depths larger than the firn–ice boundary depth, h_c (triangles). All data on ^{14}C are corrected for radioactive decay. The vertical line marks the ice age at the firn–ice boundary (t_c).

ray intensity near a glacier surface depends on two factors: (1) the intensity of primary cosmic rays in the near-Earth space, i.e., the solar activity level and geomagnetic field and (2) the thickness of the atmosphere above a glacier, i.e., the atmospheric pressure and glacier height above sea level. For geomagnetic latitudes of $\lambda > 60°$, the geomagnetic field is not a governing factor. At large depths, radiocarbon is produced in the reactions caused by the cosmic ray muon component. The muon flux is weakly sensitive to the possible changes in the glacier height or atmospheric pressure: a change in a glacier height of 3.5 km by 10% corresponds to a change in the muon component flux by 3% (Fig. 2). The muon flux is also weakly sensitive to the

possible variations in the solar activity level; e.g., according to the data of the Nagoya muon telescope (35° N, 137° E), the amplitude of the muon flux variations was 10−15% during solar cycle 22 (1986−1996) [Storini and Laurenza, 2003]. Thus the anticipated concentration error, caused by the possible past variations in the muon component flux, is smaller than the reaction cross section error.

5. CONCLUSIONS

We considered the radiocarbon production in a glacier body by the cosmic radiation. The contribution of the cosmic radiate muon component to the radiocarbon production process is not negligible, and the characteristic production depth is several tens of mwa. The radiocarbon production by the cosmic ray muon components should be taken into account during an analysis and interpretation of experimental data. The experimental values of the ^{14}C concentration in deep ice samples from the Vostok and Taylor Dome boreholes can be explained by the radiocarbon production in the reactions caused by the cosmic radiation muon component.

REFERENCES

D. Desilets and M. Zreda, "Spatial and Temporal Distribution of Secondary Cosmic-Ray Nucleon Intensities and Applications to in situ Cosmogenic Dating," Earth Planet. Sci. Lett. **206**, 21−42 (2003).

D. Desilets, M. Zreda, and T. Prabu, "Extended Scaling Factors for in situ Cosmogenic Nuclides: New Measurements at Low Latitude," Earth Planet. Sci. Lett. **246**, 265−276 (2006).

P. M. Grootes, E. J. Steig, M. Stuiver, et al., "A New Ice Core Record from Taylor Dome, Antarctica, EOS Trans. **75**, 225 (1994).

B. Heisinger, D. Lal, A. J. T. Jull, et al., "Production of Selected Cosmogenic Radionuclides by Muons, 1: Fast Muons," Earth Planet. Sci. Lett. **200**, 345−355 (2002a)

B. Heisinger, D. Lal, A. J. T. Jull, et al., "Production of Selected Cosmogenic Radionuclides by Muons, 2: Capture of Negative Muons," Earth Planet. Sci. Lett. **200**, 357−369 (2002b).

J. Jouzel et al., "Extending the Vostok Ice-Core Record of Paleoclimate to the Penultimate Glacial Period," Nature **364**, 407−412 (1993).

A. J. T. Jull, N. Lifton, W. M. Phillips, and J. Quade, "Studies of the Production Rate of Cosmic-Ray Produced ^{14}C in Rock Surfaces," Nucl. Instr. Meth. B **92**, 308−310 (1994).

D. Lal, A. J. T. Jull, D. J. Donahue, et al., "The Record of Cosmogenic in situ Produced ^{14}C in Vostok and Taylor Dome Ice Samples: Implications for Strong Role of Wind Ventilation Processes," J. Geophys. Res. **106D**, 31 933−31 941 (2001).

D. Lal, A. J. T. Jull, D. Pollard, and L. Vacher, "Evidence for Large Century Time-Scale Changes in Solar Activity in the Past 32 kyr, Based on in situ Cosmogenic ^{14}C in Ice at Summit, Greenland," Earth Planet. Sci. Lett. **234**, 335−349 (2005).

D. Lal, "Cosmic Ray Labeling of Erosion Surfaces: In situ Nuclide Production Rates and Erosion Models," Earth Planet. Sci. Lett. **104**, 424−439 (1991).

D. F. Measday, "The Nuclear Physics of Muon Capture," Phys. Rep. **354**, 243−409 (2001).

E. Monnin et al., "Evidence for Substantial Accumulation Rate Variability in Antarctica during the Holocene, through Synchronization of CO_2 in the Taylor Dome C and DML Ice Cores," Earth Planet. Sci. Lett. **224**, 45−54 (2004).

J. R. Petit et al., "Climate and Atmospheric History of the Past 420 000 Years from the Vostok Ice Core, Antarctica," Nature **399**, 429−436 (1999).

N. Reeh, "The Age−Depth Profile in the Upper Part of a Steady-State Ice Sheet," J. Glaciol. **35** (121), 406 (1989).

A. N. Salamatin and V. Ya. Lipenkov, "Simple Relations for the Close−Off Depth and Age in Dry-Snow Densification," Ann. Glaciol. **49**, 71−76 (2008).

A. M. Smith, V. A. Levchenko, D. M. Etheridge, et al., "In Search of in situ Radiocarbon in Low Dome Ice and Firn," Nucl. Instr. Meth. B **172**, 610−622 (2000).

E. J. Steig, E. J. Brook, J. W. C. White, et al., "Synchronous Climate Changes in Antarctica and North Atlantic Activity," Science **282**, 92−95 (1998).

M. Storini and M. Laurenza, "Solar Effects on Muon Data," Mem. S. A. It. **74**, 774 (2003).